SurfATT: High-Performance Package for Adjoint-State Surface-Wave Travel-Time Tomography

Mijian Xu[1] , Shijie Hao[1] , Jing Chen[1] , Bingfeng Zhang[1] , and Ping Tong[*1,2,3]

Abstract

SurfATT is a novel software package designed for ambient noise surface-wave tomography. It employs the innovative adjoint-state travel-time tomography method with the consideration of model inhomogeneity and surface topography. Key features of SurfATT include a user-friendly interface, efficient memory utilization, and high computational performance. As a result, it capably handles surface-wave tomography for large-scale datasets and models. Benchmark tests further highlight SurfATT's remarkable performance, particularly on high-performance computing systems and Apple M1 Max chip, underscoring its potential compatibility across diverse computing environments. Its application to the western U.S. region showcases its effectiveness in generating high-resolution tomographic images and revealing spatial correlations with tectonic features. Overall, SurfATT emerges as an efficient solution for surface-wave tomography tasks, offering researchers and practitioners a powerful tool for understanding Earth's subsurface structures.

Introduction

Surface-wave travel-time tomography using ambient noise data has been demonstrated as an efficient method for imaging *S*-wave velocity in the crust (e.g., Shapiro *et al.*, 2005; Fang *et al.*, 2015). Our preceding studies proposed an innovative technique called adjoint-state travel-time tomography (ATT) to compute sensitivity kernels of travel time, and to iteratively optimize model parameters of velocity and anisotropy (Tong, 2021a,b; Chen, Chen, *et al.*, 2023). Applications to body-wave tomography using the ATT method have exhibited refined velocity and anisotropic structures in the crust and upper mantle, illuminated by regional and teleseismic travel times (Wang *et al.*, 2022; Wu *et al.*, 2022; Chen, Wu, *et al.*, 2023). Recently, we have extended the ATT method to surface-wave travel-time tomography (Hao *et al.*, 2024). By solving the eikonal equation and its adjoint equation within an inhomogeneous surface-wave velocity model at varying frequencies, the frequency-dependent travel-time field and adjoint field can be calculated. Furthermore, the effect of topography on surface-wave travel time is incorporated by solving the eikonal equation on a curved surface. By accounting for both model inhomogeneity and topography, we have improved the accuracy and reliability of surface-wave travel-time tomography across scales ranging from local to continental (Hao *et al.*, 2024).

To allow researchers worldwide to utilize this innovative topography-incorporated surface-wave travel-time tomography method, we have developed a software package called SurfATT.

This software is driven by Modern Fortran with a modular design. The Message Passing Interface (MPI) technique is utilized for multilevel parallelization to enhance computational performance. To reduce memory consumption, we employ the shared memory technique for allocating memory for data, model, and kernel matrices. This package supports popular input and output file formats, such as YAML parameter files, comma-separated values (CSV) data files, and Hierarchical Data Format version 5 (HDF5) model files, to improve its user-friendliness. SurfATT is an open-source software licensed under the GNU General Public License version 3.0 (GPL v.3). We also provide online documentation powered by Sphinx (see Data and Resources). Detailed installation instructions and tutorials are available within this documentation.
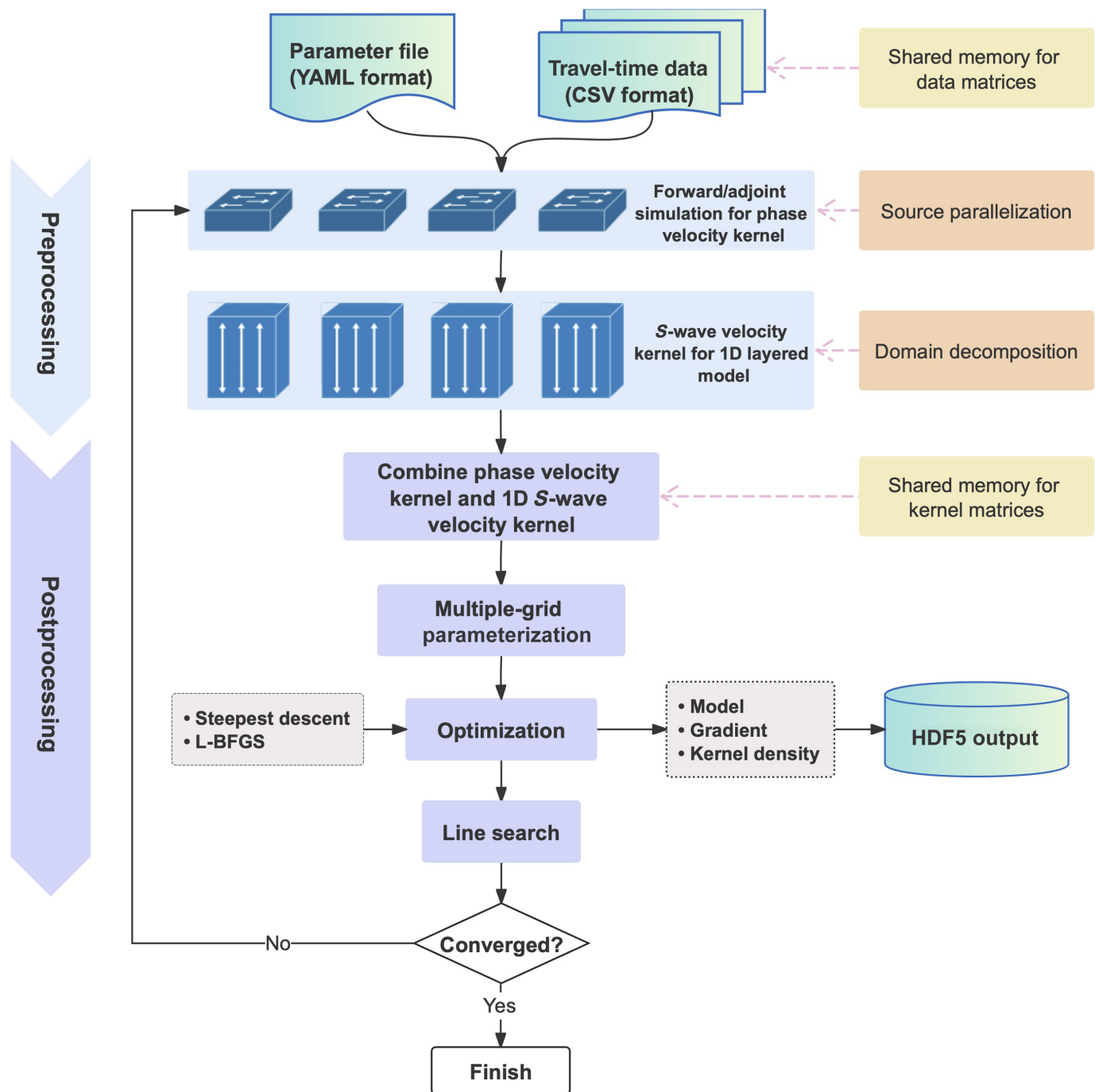
Overview of Adjoint-State Surface-Wave Travel-Time Tomography

Figure 1 demonstrates the framework of SurfATT, which implements a linearized iterative algorithm. Each iteration

1. Division of Mathematical Sciences, School of Physical and Mathematical Sciences, Nanyang Technological University, Singapore, Singapore, https://orcid.org/0000-0001-8888-8523 (MX); https://orcid.org/0000-0003-1594-3039 (SH); https://orcid.org/0000-0002-9083-3940 (JC); https://orcid.org/0000-0003-1124-3481 (BZ); https://orcid.org/0000-0002-1937-3427 (PT); 2. Earth Observatory of Singapore, Nanyang Technological University, Singapore, Singapore; 3. Asian School of the Environment, Nanyang Technological University, Singapore, Singapore

*Corresponding author: tongping@ntu.edu.sg

Figure 1. The general framework of SurfATT. The color version of this figure is available only in the electronic edition.
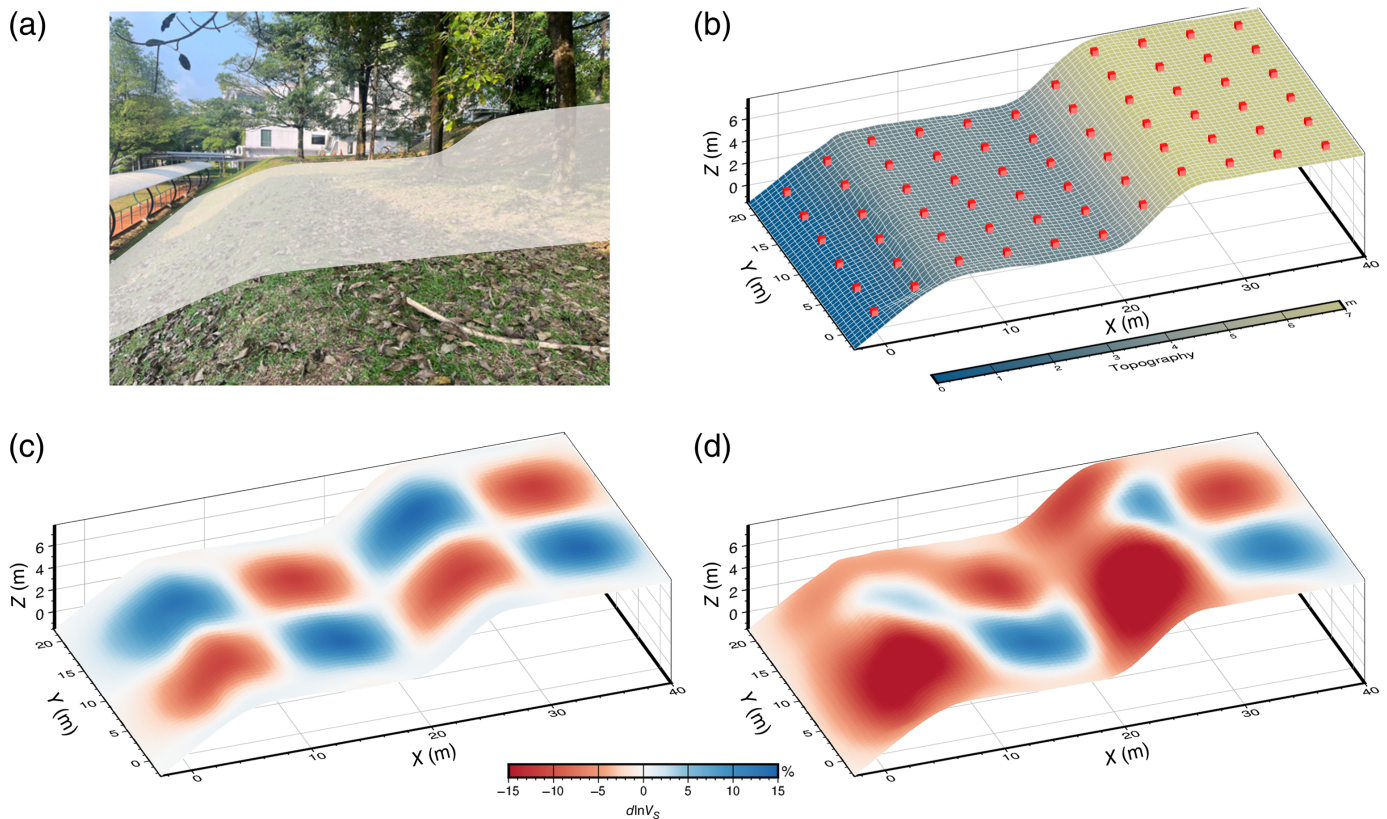
contains two primary stages. In the preprocessing stage, the forward modeling employs a 3D *S*-wave velocity model to compute phase velocity and travel times, in which phase velocities at each horizontal position are computed under the assumption of a 1D layered model (Aki and Richards, 2002). The travel-time field for each virtual source is computed by solving the eikonal equation with the fast sweeping method (FSM) (Zhao, 2005). Subsequently, we proceed to compute two types of sensitivity kernels. Note that the sensitivity kernel of the travel-time objective function regarding phase velocity (phase velocity kernel) is derived using the adjoint-state method (Hao *et al.*, 2024), and the sensitivity of phase velocity

to *S*-wave velocity (*S*-wave velocity kernel) is derived through the variational principle (Woodhouse, 1974).

The postprocessing stage involves model updating using phase velocity kernels and *S*-wave velocity kernels. At each given period, the corresponding phase velocity kernels are combined into a unified sum. The summed phase velocity kernels are then integrated with *S*-wave velocity kernels, adopting equation (22) in Hao *et al.* (2024), to derive the misfit kernel of the objective

Figure 2. (a) A photograph of the experimental area on the Nanyang Technological University campus. (b) Topography of the experimental area. The red cubes represent seismometers. The white grids represent the regular mesh with topography used in tomography. (c) Results of the checkerboard test for surface-wave tomography at 60 Hz with topography incorporated. The colors denote phase velocity anomalies relative to the initial velocity of 250 m/s. (d) The same as panel (c) but with topography excluded by setting the elevation to 0 m. The color version of this figure is available only in the electronic edition.

function concerning the 3D S-wave velocity. The multiple-grid method is employed to parameterize the S-wave velocity model on an inversion grid consisting of multiple regular coarse grids placed in a staggered arrangement (Tong *et al.*, 2019). SurfATT provides two optimization schemes of the steepest descent method and limited-memory Fletcher–Goldfarb–Shanno (L-BFGS) algorithm for updating the S-wave velocity model. For the classic steepest descent method, we compute the kernel density K_{den} by assigning a travel-time residual of -1 s to each measurement and then computing the related misfit kernel. The V_S misfit kernel is regularized by multiplying the preconditioner $\frac{1}{K_{\mathrm{den}}^N}$ as an approximation to the inverse Hessian, in which N is the exponent to rescale the kernel density. Alternatively, the L-BFGS method is available for optimization (Liu and Nocedal, 1989), in which the approximate inverse Hessian at the kth iteration is given by

$$H_k = \frac{s_{k-1}^T y_{k-1}}{y_{k-1}^T y_{k-1}} I, \tag{1}$$

in which $y_{k-1} = g_k - g_{k-1}$ is the gradient change, $s_{k-1} = m_k - m_{k-1}$ is the model change. The line search method is utilized to determine the optimal step length (Nocedal and Wright, 2006).
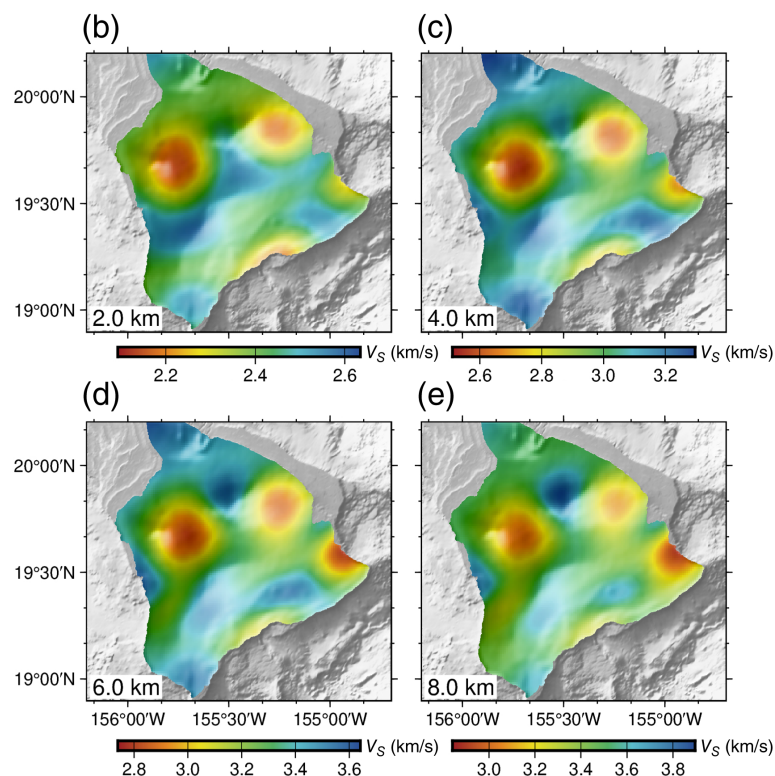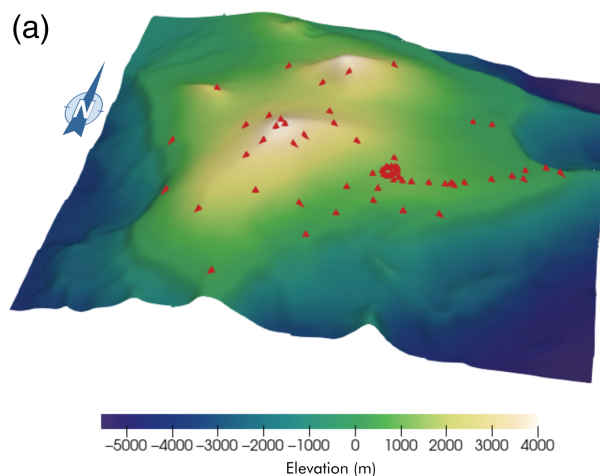
Features of SurfATT
Surface topography in consideration
Hao *et al.* (2024) propose a new method for computing phase velocity kernel by solving a 2D eikonal equation on a curved

surface. When surface waves propagate along curved surfaces with topographic variations, their travel-time fields can be modeled using an elliptical anisotropic eikonal equation. SurfATT employs this method to calculate sensitive kernels by computing the travel-time field and its adjoint field, which is then integrated into surface-wave tomography, thereby enhancing tomographic accuracy. To assess the effect of surface topography on surface-wave tomography, we conducted synthetic tests based on an experiment at Nanyang Technological University, Singapore. Within a sloped area measuring 25 m × 42.5 m on campus (Fig. 2a), we deployed 66 nodal seismometers and measured the topography within the area, ranging from 0 to 7.4 m (Fig. 2b). Using phase velocity tomography at 60 Hz as an example, we set up a checkerboard test to verify the effect of topography on tomography. When topography is considered, the patterns of all the 2 by 4 checkers can be perfectly restored (Fig. 2c); however, when the topography is neglected and set

Volume XX • Number XX • XXXX XXXX • www.srl-online.org
Seismological Research Letters **3**

Downloaded from http://pubs.geoscienceworld.org/ssa/srl/article-pdf/doi/10.1785/0220240206/7101562/srl-2024206.1.pdf
by Nanyang Technological University user

Figure 3. (a) Surface topography of the Hawaii Island and adjacent regions. The red triangles represent stations used for tomography. (b–e) S-wave velocity at depths of 2, 4, 6, and 8 km. The color version of this figure is available only in the electronic edition.

to zero, the checker patterns become difficult to restore, and the phase velocity is underestimated compared to the target model (Fig. 2d). These results demonstrate the necessity of accounting for topographic variations in surface-wave tomography, particularly in areas with significant topographic changes.

SurfATT requires surface topography data in the generic Network Common Data Form (NetCDF) format, which can be easily extracted using the "grdcut" command in the Generic Mapping Tools (GMT) (Wessel *et al.*, 2019). Here, we replicate the previous ambient noise surface-wave tomography in Hawaii Island using SurfATT (Fig. 3). The results indicate that the velocity anomalies in our imaging are highly consistent with those reported by Hao *et al.* (2024). The details of this example can be accessible in the online documentation (see Data and Resources). Because of the consideration of surface topography, SurfATT is applicable for imaging in small-scale regions with significant surface topography. Thus, this method offers potential prospects for shallow structure exploration using dense short-period arrays.

Stability and reduced parameter settings

SurfATT fully accounts for inversion stability, simpler parameter tuning, and reduced dependence on prior information benefiting from several key methodological choices. First, the method employs a line search to determine the optimal step size in each iteration, thus eliminating the need for damping adjustment, often required by other linear solvers and chosen by the L-curve method (Rawlinson and Sambridge, 2003). This approach simplifies parameter tuning and avoids inconsistencies

in inversion results that could arise from varying damping values. In addition, the initial model is derived from a 1D inversion of the averaged dispersion curve, which reduces the inversion's nonlinearity and is particularly advantageous at regional scales, where it effectively eliminates the need for additional initial models, streamlining the setup. To approximate the inverse Hessian, SurfATT employs the L-BFGS optimization to approximate the inverse Hessian, which reduces the necessity for additional regularization. The main user-defined factor impacting inversion results is the choice of inversion grid spacing, which controls the smoothness of the sensitivity kernels. Based on the checkerboard test, we recommend setting 3–5 grid points per anomaly, aligning with the minimum resolvable anomaly size for optimal resolution.

User-friendliness

To ensure user-friendly accessibility and streamlined functionality, SurfATT incorporates a range of features. The use of CMake for compilation simplifies the build process and enhances user-friendliness by providing a platform-independent build system. CMake automates the generation of build files for various development environments, allowing users to compile SurfATT effortlessly on their preferred platform.

SurfATT focuses on enhancing user-friendliness by employing widely accepted data formats such as CSV for travel-time data storage, YAML Ain't Markup Language (YAML) for input parameter configuration, HDF5 for model organization, and Network Common Data Form (NetCDF format) for surface topography. These formats are chosen for their readability, ease of parsing, and cross-platform compatibility, ensuring that users can easily handle and exchange data and parameters across different environments and platforms.

In addition, the inversion process is seamlessly integrated into a single command to streamline the workflow and minimize user input requirements. By encapsulating the inversion procedure within a single command, users can initiate the entire process with just two or three input files (input parameters, travel-time data, or/and surface topography), reducing complexity and enhancing usability. This integration simplifies the execution of surface-wave travel-time tomography and facilitates a more user-friendly experience for researchers.

Low memory consumption

The adjoint method offers a significant advantage in seismic imaging by enabling the summation of sensitivity kernels for each seismic event without the need to allocate coefficient matrices as required in solving linear equation systems. This approach dramatically reduces memory consumption, making it particularly advantageous for large-scale datasets and memory-constrained environments (e.g., laptop and personal computer PC). This memory-efficient strategy enhances computational performance and scalability, making SurfATT an ideal choice for processing massive datasets with limited memory resources.

SurfATT employs a shared memory technique based on MPI to enable multiple processors to read variables from a single physical memory. This approach significantly reduces memory consumption by allowing concurrent access to shared resources, including travel-time data, velocity models, sensitivity kernels, and other memory-intensive variables. Moreover, SurfATT utilizes different MPI communicators to implement shared memory across multiple physical nodes. By organizing processors into different communicators, SurfATT facilitates efficient memory sharing among processors residing on different physical nodes. This distributed memory architecture enhances scalability and performance, and hence enables SurfATT to handle large-scale datasets across various computing environments.

High performance

SurfATT utilizes the FSM to solve the elliptically anisotropic eikonal equation (Luo and Qian, 2011; Tong, 2021b), offering significant advantages in accuracy and efficiency. First, this method is proven to unconditionally converge to the realistic travel-time field of first arrivals (Zhao, 2005). By applying the multiplicative factorization technique (Luo and Qian, 2011), numerical errors caused by source singularity can be eliminated to ensure the accuracy of the FSM. In addition, the
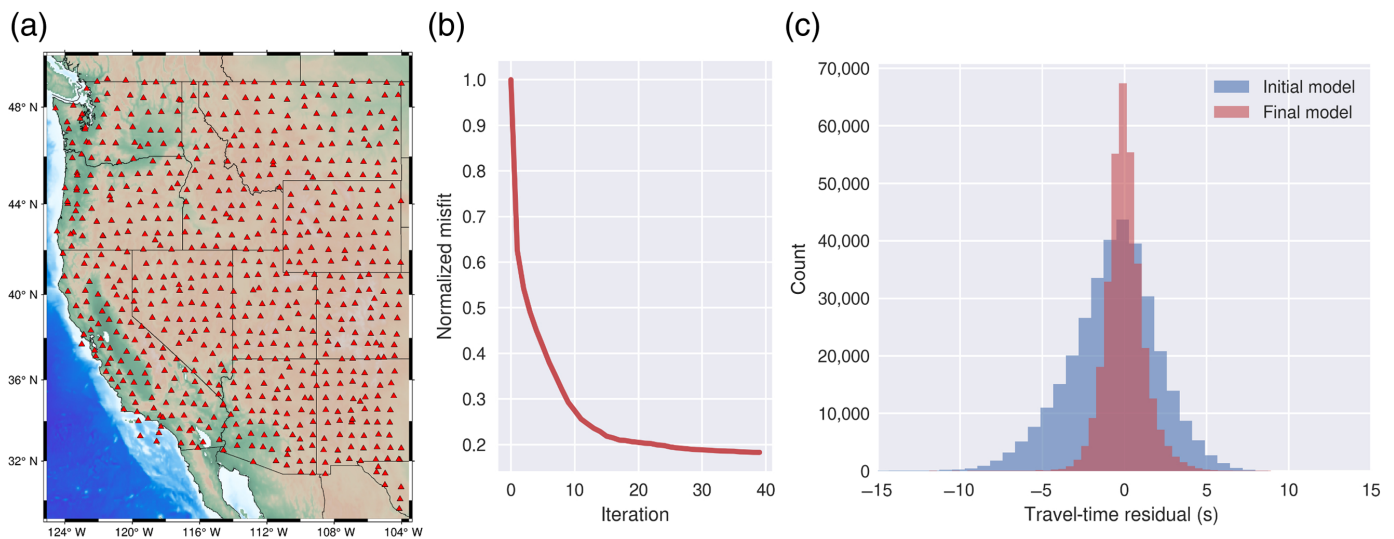
FSM achieves optimal computational complexity of O(N), in which N denotes the total number of grid points. This results in higher efficiency compared to other approaches, such as the fast marching method with O($N\log N$) computational complexity (Zhao, 2005), especially when considering large study regions discretized on numerous gird nodes.

SurfATT implements multilevel parallelization to maximize its computational efficiency, thanks to the independence of computing 2D phase velocity kernels and 1D S-wave velocity kernels. For 2D phase velocity kernels, event parallelization is employed to distribute the computation of the 2D eikonal equation and its adjoint equation across multiple processors. Each seismic event is processed independently, allowing concurrent computation of sensitivity kernels. On the other hand, SurfATT utilizes domain decomposition techniques to partition the computational domain into smaller subdomains, each processed independently in parallel. Within each subdomain, we traverse each surface grid point to calculate its S-wave velocity kernel. The multilevel parallelization approach in SurfATT enables efficient utilization of parallel processing resources to achieve high-performance computing (HPC) capabilities for large-scale datasets and study regions.

Example in the Western United States

In the western U.S. region, we apply SurfATT to a phase velocity dispersion dataset extracted from ambient noise in the USArray database (Ekström, 2014). A total of 689 stations are selected within the coordinates of 125°–104° W and 29°–49° N (Fig. 4a), resulting in 334,555 rays from 7,454 virtual sources. The area is discretized into a mesh with intervals of 0.1° × 0.1° × 2 km, generating a total of 1,824,336 grid points. The adjoint-state surface-wave travel-time tomography is conducted on an HPC using 192 processors powered by two Intel Xeon Platinum 9242 central processing units (CPUs). Remarkably, only 868 s is needed for 40 iterations with the L-BFGS optimization method and only 14 GB of memory is utilized during this inversion. After 40 iterations, the misfit is reduced by ∼80% (Fig. 4b). The mean value of the travel-time residuals changes from −0.7181 to 0.0181 s, and the standard deviation decreases from 2.8966 to 1.2764 s (Fig. 4c).

In addition, during parallel computation of the phase velocity kernels, a memory of size M is allocated for the sensitivity kernels on each processor, leading to a total memory consumption of $M \times N$, in which N is the number of processors. Therefore, using fewer processors would result in smaller memory consumption. To evaluate both the memory consumption and performance with fewer processors, we conduct surface-wave tomographic inversion for the western U.S. case with eight processors on the Apple M1 Max chip. The inversion process demonstrates remarkable performance, completing 40 iterations in a total computation time of 6527 s. Notably, only 2.9 GB of memory is utilized during the inversion, indicating efficient memory consumption. Despite the longer

(a) **(b)** **(c)**

Figure 4. (a) Topographic map view of the western United States. The red triangles denote stations in the phase velocity dispersion dataset (Ekström, 2014). The black lines denote tectonic boundaries. (b) Misfit reduction over iterations. (c) Histogram of travel-time residuals. The blue and red bars represent distributions of travel-time residuals in the initial and final models, respectively. The color version of this figure is available only in the electronic edition.

absolute computational time, the overall efficiency on the Apple M1 Max chip exceeds that of common HPC systems. This can be attributed to the optimized architecture and design of the Apple M1 chip, which integrates high-performance CPU and unified memory architecture. This case study in the western United States is executed on both HPC and PC platforms, demonstrating excellent computational efficiency, as well as the excellent cross-platform performance of SurfATT.

Benchmark tests are conducted to evaluate the speed-up achieved by SurfATT with an increasing number of processors. The results show a significant speed-up performance (Fig. 5), with 96 processors achieving ~90% of maximum acceleration scaling compared to serial execution. With 192 processors, the acceleration scaling ranges between 70% and 80% of the maximum scaling. However, the proportion of time spent on interprocessor data exchange increases with the number of processors. This is a significant factor contributing to the decrease in the acceleration scaling. In this example, the computation time for calculating the phase velocity kernels on 192 processors is 6.3 s, whereas the computation time for calculating the S-wave velocity kernel is 1.5 s. However, the interprocessor data exchange requires ~0.5 s, resulting in a significant proportion of the overall computation time being dedicated to data exchange. Thus, we infer that with denser grids and larger-scale datasets, the acceleration is expected to be higher than observed in this test due to a decreased proportion of interprocessor data exchange.

Checkerboard tests can be easily conducted using the SurfATT package. The built-in command "`surfatt_cb_fwd`" facilitates the creation of a checkerboard model and performs forward simulation to obtain synthetic travel-time data. Random noise can be assigned to the synthetic data to simulate realistic conditions. Once the synthetic travel-time data are generated, the same inversion strategy used for observed data can be applied to obtain the result of the checkerboard test. Figure 6 shows the results of a checkerboard test for this USArray dataset. The checkerboard

pattern is well recovered across the American continent, with resolution extending down to 80 km depth.

Figure 7 demonstrates the crustal and upper-mantle S-wave velocity. In the shallow crust, low-velocity anomalies are observed beneath typical sedimentary basins and volcanic areas, including the Great Valley, the Columbia River Basin, and the Yellowstone. Conversely, high-velocity features are
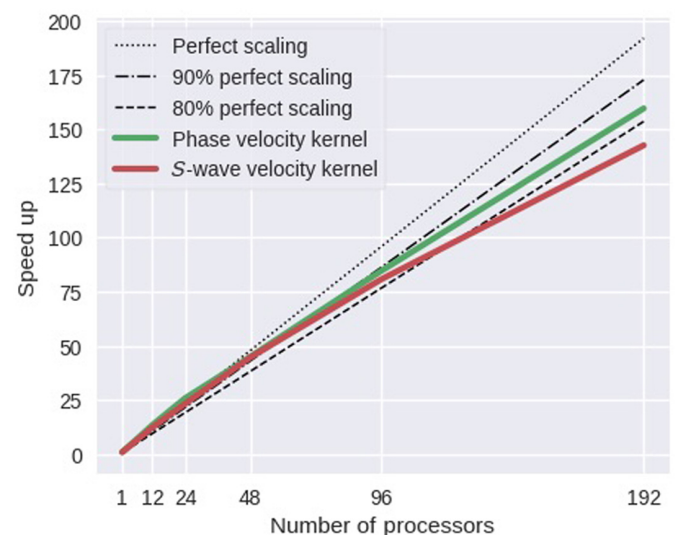
Figure 5. Speed-up scaling against the number of processors. The color version of this figure is available only in the electronic edition.
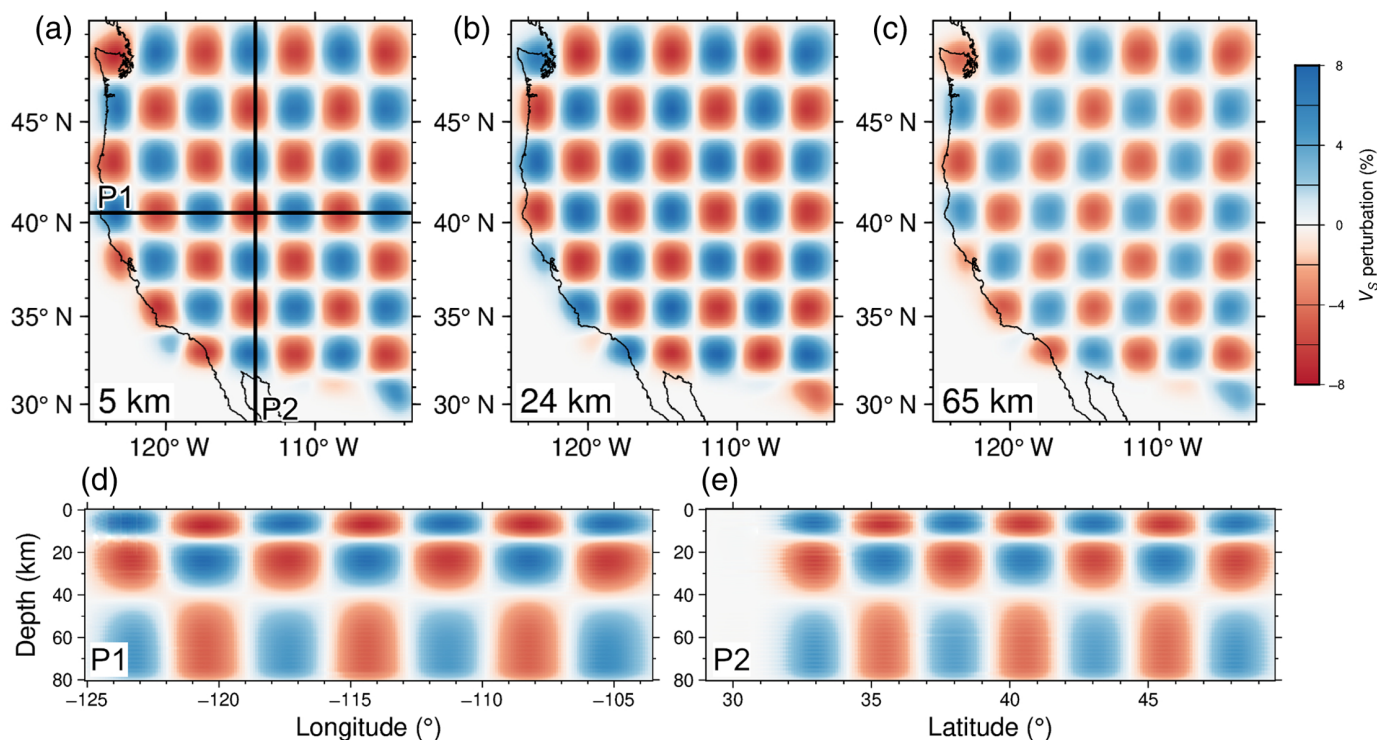
Figure 6. (a–c) Map view of checkerboard resolution test results at 5, 24, and 65 km depth. (d,e) Results along profiles P1 and P2. The color version of this figure is available only in the electronic edition.

prevalent in the orogeny and plateau regions, such as the Sierra Nevada, the Columbia Plateau, and the Colorado Plateau. In the middle crust, low-velocity zones are found beneath the Basin and Range, including the Great Basin and the Southern Basin and Range. These observations are consistent with previous tomographic findings (Schmandt *et al.*, 2015).

In the upper mantle, imaging at 50 km depth reveals normal-to-high velocity of 4.4–4.5 km/s in the Columbia Plateau, southern California, and the Basin and Range (Fig. 7c). In contrast, a low-velocity zone of 4.0–4.2 km/s is observed beneath the Basin and Range at a depth of 65 km (Fig. 7d). These features align with previous tomographic studies (e.g., Yang *et al.*, 2008; Schmandt *et al.*, 2015). Receiver function observations have indicated a lithospheric thickness of ∼60 km in southern California and the Basin and Range (Lekić *et al.*, 2011; Lekić and Fischer, 2014). Thus, the normal-to-high velocity at 50 km depth symbolizes the lithosphere, whereas the low-velocity zone at 65 km depth signifies the asthenosphere. In summary, the tomographic results obtained using SurfATT exhibit a strong spatial correlation with tectonic blocks and demonstrate consistency with previous *S*-wave velocity structures. This highlights SurfATT's capability to generate robust tomographic results and to provide valuable insights into subsurface structures.

Future Works

SurfATT is designed as a cross-platform and open-source software, and we encourage the community to contribute to its development by submitting feature requests. In future iterations of SurfATT, we aim to expand the software's capabilities

in several key areas. Based on the azimuthal anisotropy sensitivity kernels for surface waves (Montagner and Nataf, 1986; Liu *et al.*, 2019) and the travel-time sensitivity kernels for anisotropic media (Tong, 2021b), we plan to extend SurfATT to incorporate both azimuthal anisotropy and travel-time sensitivity in anisotropic media. This development will enable more accurate modeling of structural heterogeneities. Currently, SurfATT employs the propagator matrix method for phase velocity computation; however, this approach would be unstable for calculating higher-mode surface waves. To address this, we intend to integrate a surface-wave solver based on numerical methods (e.g., spectrum element method), which will improve stability and enable robust imaging utilizing higher-mode surface waves in future releases.

Conclusion

In conclusion, SurfATT offers a robust solution for surface-wave travel-time tomography, characterized by user-friendliness, low memory usage, high performance, and reliability. By leveraging CSV data, YAML parameters, and HDF5 storage, SurfATT streamlines data handling and parameter configuration for users. Its implementation of the adjoint method and shared memory techniques optimizes memory usage and computational efficiency, whereas the advanced FSM and multilevel
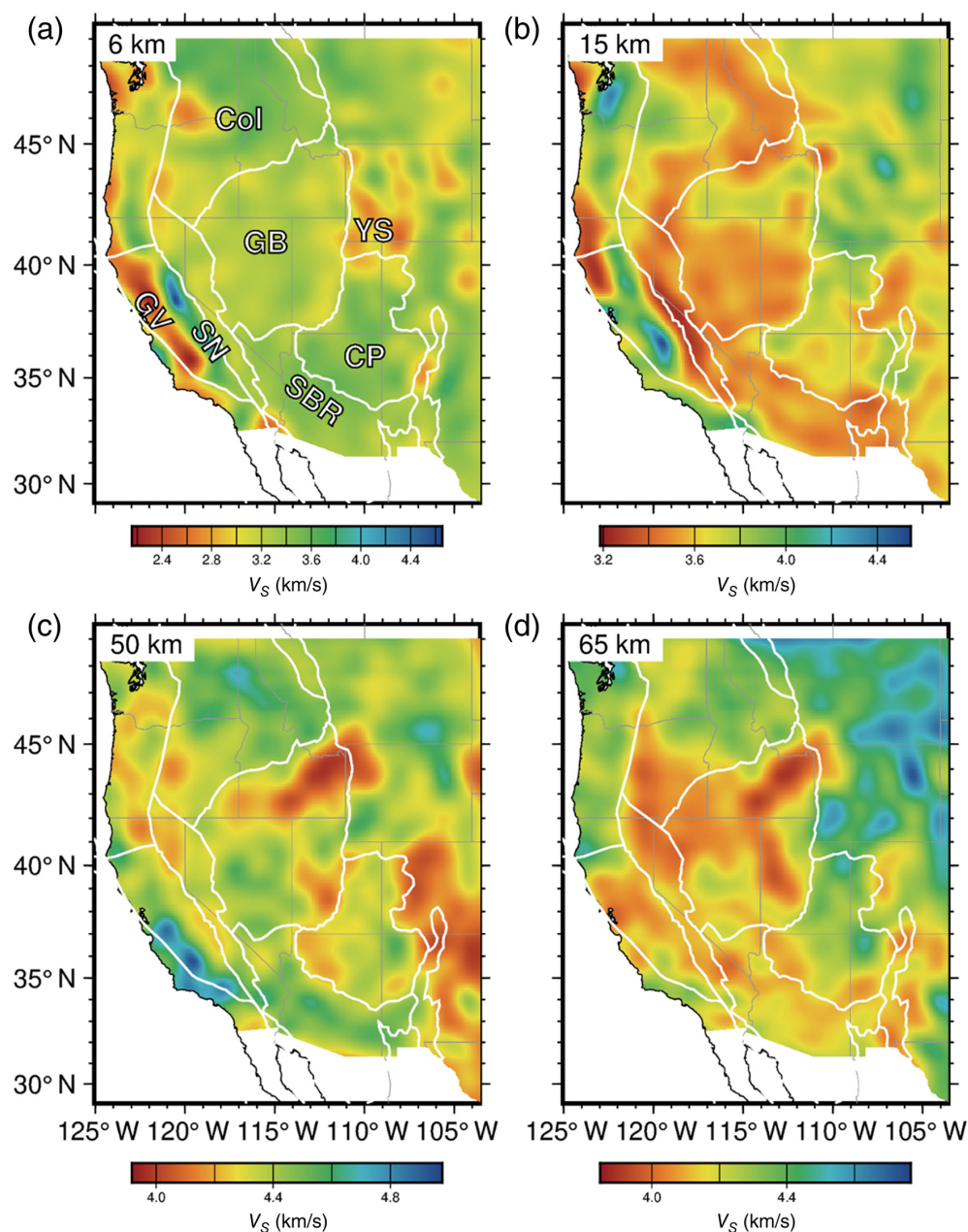
Figure 7. Map views of *S*-wave velocity at depths of (a) 6, (b) 15, (c) 50, and (d) 65 km. Geologic abbreviations: CP, Colorado plateau; Col, Columbia plateau; GB, Great Basin; GV, Great Valley; SBR, southern Great Basin; SN, Sierra Nevada; and YS, Yellowstone. The color version of this figure is available only in the electronic edition.

parallelization strategies enhance scalability and performance. The successful application of SurfATT to the western U.S. region demonstrates its efficacy in generating reliable tomographic results, showcasing strong spatial correlations with tectonic blocks. Furthermore, benchmark tests highlight SurfATT's remarkable performance on both PCs and HPC systems, underscoring its versatility and effectiveness across diverse computing architectures. Overall, SurfATT offers comprehensive solutions for surface-wave travel-time tomography tasks.

References

Aki, K., and P. G. Richards (2002). *Quantitative Seismology*, University Science Books, Sausalito, California.

Chen, J., G. Chen, M. Nagaso, and P. Tong (2023). Adjoint-state traveltime tomography for azimuthally anisotropic media in spherical coordinates, *Geophys. J. Int.* **234,** no. 1, 712–736, doi: 10.1093/gji/ggad093.

Chen, J., S. Wu, M. Xu, M. Nagaso, J. Yao, K. Wang, T. Li, Y. Bai, and P. Tong (2023). Adjoint-state teleseismic traveltime tomography: method

and application to Thailand in Indochina Peninsula, *J. Geophys. Res.* **128,** no. 12, e2023JB027348, doi: 10.1029/2023JB027348.

Ekström, G. (2014). Love and Rayleigh phase-velocity maps, 5–40 s, of the western and central USA from USArray data, *Earth Planet. Sci. Lett.* **402,** 42–49, doi: 10.1016/j.epsl.2013.11.022.

Fang, H., H. Yao, H. Zhang, Y.-C. Huang, and R. D. Van Der Hilst (2015). Direct inversion of surface wave dispersion for three-dimensional shallow crustal structure based on ray tracing: Methodology and application, *Geophys. J. Int.* **201,** no. 3, 1251–1263.

Hao, S., J. Chen, M. Xu, and P. Tong (2024). Topography-incorporated adjoint-state surface wave traveltime tomography: Method and a case study in Hawaii, *J. Geophys. Res.* doi: 10.1029/2023JB027454.

Herrmann, R. B. (2013). Computer programs in seismology: An evolving tool for instruction and research, *Seismol. Res. Lett.* **84,** no. 6, 1081–1088, doi: 10.1785/0220110096.

Komatitsch, D., and J. Tromp (2002a). Spectral-element simulations of global seismic wave propagation-I. Validation, *Geophys. J. Int.* **149,** no. 2, 390–412, doi: 10.1046/j.1365-246X.2002.01653.x.

Komatitsch, D., and J. Tromp (2002b). Spectral-element simulations of global seismic wave propagation-II. Three-dimensional models, oceans, rotation and self-gravitation, *Geophys. J. Int.* **150,** no. 1, 303–318, doi: 10.1046/j.1365-246X.2002.01716.x.

Lekić, V., and K. M. Fischer (2014). Contrasting lithospheric signatures across the western United States revealed by Sp receiver functions, *Earth Planet. Sci. Lett.* **402,** 90–98, doi: 10.1016/j.epsl.2013.11.026.

Lekić, V., S. W. French, and K. M. Fischer (2011). Lithospheric thinning beneath rifted regions of southern California, *Science* **334,** no. 6057, 783–787, doi: 10.1126/science.1208898.

Liu, C., H. Yao, H. Yang, W. Shen, H. Fang, S. Hu, and L. Qiao (2019). Direct inversion for three-dimensional shear wave speed azimuthal anisotropy based on surface wave ray tracing: Methodology and application to Yunnan, Southwest China, *J. Geophys. Res.* **124,** no. 11, 11,394–11,413, doi: 10.1029/2018JB016920.

Liu, D. C., and J. Nocedal (1989). On the limited memory BFGS method for large scale optimization, *Math. Program.* **45,** no. 1, 503–528, doi: 10.1007/BF01589116.

Luo, S., and J. Qian (2011). Factored singularities and high-order Lax–Friedrichs sweeping schemes for point-source traveltimes and amplitudes, *J. Comput. Phys.* **230,** no. 12, 4742–4755, doi: 10.1016/j.jcp.2011.02.043.

Montagner, J.-P., and H.-C. Nataf (1986). A simple method for inverting the azimuthal anisotropy of surface waves, *J. Geophys. Res.* **91,** no. B1, 511, doi: 10.1029/JB091iB01p00511.

Nocedal, J., and S. J. Wright (2006). *Numerical Optimization,* Springer Series in Operations Research, Springer, New York.

Rawlinson, N., and M. Sambridge (2003). Seismic traveltime tomography of the crust and lithosphere, in *Geohazards,* C. Schmelzbach (Editor), Advances in Geophysics, Vol. 46, Elsevier, London, United Kingdom.

Schmandt, B., F. Lin, and K. E. Karlstrom (2015). Distinct crustal isostasy trends east and west of the Rocky Mountain Front, *Geophys. Res. Lett.* **42,** no. 23, doi: 10.1002/2015GL066593.

Shapiro, N. M., M. Campillo, L. Stehly, and M. H. Ritzwoller (2005). High-resolution surface-wave tomography from ambient seismic noise, *Science* **307,** no. 5715, 1615–1618, doi: 10.1126/science.1108339.

Tong, P. (2021a). Adjoint-state traveltime tomography: Eikonal equation-based methods and application to the Anza Area in Southern California, *J. Geophys. Res.* **126,** no. 5, doi: 10.1029/2021JB021818.

Tong, P. (2021b). Adjoint-state traveltime tomography for azimuthally anisotropic media and insight into the crustal structure of Central California Near Parkfield, *J. Geophys. Res.* **126,** no. 10, doi: 10.1029/2021JB022365.

Tong, P., D. Yang, and X. Huang (2019). Multiple-grid model parametrization for seismic tomography with application to the San Jacinto fault zone, *Geophys. J. Int.* **218,** no. 1, 200–223, doi: 10.1093/gji/ggz151.

Wang, K., S. Wu, and P. Tong (2022). Crustal deformation in the Sierra Nevada and walker lane region inferred from P-wave Azimuthal anisotropy, *J. Geophys. Res.* **127,** no. 12, e2022JB024554, doi: 10.1029/2022JB024554.

Wessel, P., J. F. Luis, L. Uieda, R. Scharroo, F. Wobbe, W. H. F. Smith, and D. Tian (2019). The Generic Mapping Tools Version 6, *Geochem. Geophys. Geosys.* **20,** no. 11, 5556–5564, doi: 10.1029/2019GC008515.

Woodhouse, J. H. (1974). Surface waves in a laterally varying layered structure, *Geophys. J. Int.* **37,** no. 3, 461–490, doi: 10.1111/j.1365-246X.1974.tb04098.x.

Wu, S., C. Jiang, V. Schulte-Pelkum, and P. Tong (2022). Complex patterns of past and ongoing crustal deformations in southern California revealed by seismic azimuthal anisotropy, *Geophys. Res. Lett.* **49,** no. 15, doi: 10.1029/2022GL100233.

Yang, Y., M. H. Ritzwoller, F.-C. Lin, M. P. Moschetti, and N. M. Shapiro (2008). Structure of the crust and uppermost mantle beneath the western United States revealed by ambient noise and earthquake tomography, *J. Geophys. Res.* **113,** no. B12, doi: 10.1029/2008JB005833.

Zhao, H. (2005). A fast sweeping method for Eikonal equations, *Math. Comput.* **74,** no. 250, 603–627.